First-principles multiphase equation of state of carbon under extreme conditions

Alfredo A. Correa
Department of Physics, University of California at Berkeley, Berkeley, California 94720, USA
and H Division, Physical Sciences Directorate, Lawrence Livermore National Laboratory, Livermore, California 94550, USA

Lorin X. Benedict, David A. Young, and Eric Schwegler
H Division, Physical Sciences Directorate, Lawrence Livermore National Laboratory, Livermore, California 94550, USA

Stanimir A. Bonev
Department of Physics, Dalhousie University, Halifax, Nova Scotia, Canada B3H 3J5
(Received 1 February 2008; revised manuscript received 19 May 2008; published 1 July 2008)

We describe the construction of a multiphase equation of state for carbon at extreme pressures based on *ab initio* electronic structure calculations of two solid phases (diamond and BC8) and the liquid. Solid-phase free energies are built from knowledge of the cold curves and phonon calculations, together with direct *ab initio* molecular-dynamics calculations of the equation of state, which are used to extract anharmonic corrections to the phonon free energy. The liquid free energy is constructed based on results from molecular-dynamics calculations and constraints determined from previously calculated melting curves, assuming a simple solidlike free-energy model. The resulting equation of state is extended to extreme densities and temperatures with a Thomas Fermi-based free-energy model. Comparisons to available experimental results are discussed.

DOI: 10.1103/PhysRevB.78.024101 PACS number(s): 81.30.Dz, 91.60.Fe, 91.60.Gf, 91.30.Mv

I. INTRODUCTION

The equation of state (EOS) of carbon at high pressure is of great interest for understanding the physics and chemistry of monatomic substances in general and has become especially relevant in recent years as a number of dynamic high-pressure experiments have been performed which explore states of matter in these conditions.[1–3] In addition, several important applications have emerged where a detailed understanding of the properties of carbon under extreme conditions is critical, such as in the design of fusion capsules for the National Ignition Facility.[4]

The design of dynamic high-pressure experiments requires the use of hydrodynamic simulations, in which materials are subjected to large pressure and temperature gradients, and the resulting response of the materials is computed with the relevant fluid transport equations.[5] The accuracy of hydrodynamic simulations depends critically on the quality of the EOS tables, as well as other constitutive relations they use as input. In addition, for a very accurate accounting of the flow of heat during dynamic compression, attention must be paid to the latent heat resulting from phase transitions.

The properties of carbon under extreme pressure and temperature conditions are also needed to devise the models of outer planets (e.g., Neptune and Uranus),[6–9] white dwarf atmospheres,[10–12] and their interiors[13,14] as well as extrasolar carbon planets.[15,16] In the context of planetary science, Ross[6] and Hubbard[7] suggested the possibility of finding elemental carbon in its diamond form in the inner layers of Uranus and Neptune, forming from the presence of methane. Benedetti *et al.*[8] reported experimental findings that methane can dissociate into diamond in the above mentioned planets. Contrary to these findings, simulations by Ghiringhelli *et al.*[9] indicate that the rate of dissociation would be extremely slow in Uranus and Neptune (but still possible in white dwarf stars). Resolving these issues requires a good understanding of the phase diagram and the equation of state of the phases involved.

This in turn means that a thermodynamically consistent *multiphase* EOS, which takes into account all known phases of the material and provides a consistent description of the equilibrium phase diagram,[17] is required. The only high-pressure phases of carbon[18] identified conclusively in experiment to date are the diamond phase, and of course the liquid. However, there is strong theoretical evidence for a higher-pressure solid phase, BC8 (body-centered cubic with eight atoms per cell), stable above a pressure of roughly 1100 GPa.[19] Such conditions are currently unattainable in static high-pressure experiments, where the best *in situ* diagnostics can be applied. First-principles simulations provide an alternate way to investigate the detailed phase-dependent properties of the system at these extreme conditions. They do not make use of empirical parameters and have been shown to have predictive power at extreme pressures.[20]

There have been numerous attempts to construct multiphase EOS models for carbon, all of which have their merits. The models of Kerley and Chhabildas,[21] van Thiel and Ree,[22] and Molodets[23] focus on the lower-pressure properties (including the graphite phase) and treat the diamond melting curve with a Lindemann-type law, which produces melting temperatures that increase monotonically with pressure. Bundy *et al.*[24] constructed a phase diagram by extrapolating a large number of lower-pressure experimental results to high temperature, also producing a diamond melting line that increases with pressure. The current understanding of the diamond melting line is that it has a maximum as a function of pressure,[25–27] which has been confirmed experimentally.[28] This behavior is accounted for in newer multiphase EOS models,[29,30] though only a limited amount of information on the properties of the liquid were included. Furthermore, to

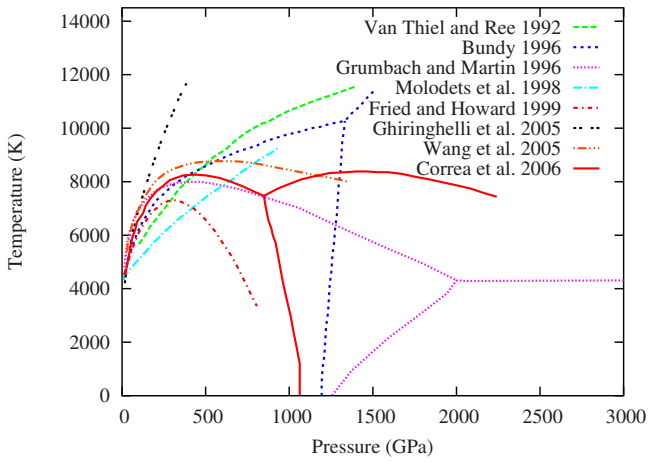

FIG. 1. (Color online) Several carbon phase diagrams proposed in the last decade, some of which include the BC8 phase. The bold line indicates phase boundaries used in this work for the construction of the liquid EOS.

the best of our knowledge, there are no multiphase EOS models for carbon that include the high-pressure BC8 phase. Several of the high-pressure carbon phase diagrams produced over recent years are displayed in Fig. 1.

In this work, we provide a multiphase EOS for elemental carbon at high pressure, which includes the three phases: diamond, BC8, and liquid. We focus specifically on an accurate description of the EOS in the range of conditions relevant in dynamic compression, such as in shock melting. The EOS is expressed as analytic functions for the free energy of the individual phases,[29,30] determined by fitting directly to the results of our *ab initio* calculations. Two types of information have been obtained from our first-principles electronic structure calculations: (1) single-phase properties, such as internal energies, pressures, and vibrational and electronic excitations, and (2) phase boundaries. The solid (diamond, BC8)-to-liquid phase lines have been determined previously using first-principles two-phase simulations.[27] The free energies of the solid phases are then obtained using what amounts to a Mie-Grüneisen model at high-T (above the Debye temperature), with additional corrections accounting for zero-point motion and anharmonic corrections. In the case of the liquid, the situation is much more complex because of the lack of a universal liquid EOS. Here we use (and validate) a model previously suggested[31,32] for monatomic systems. We show how the knowledge of the melting line, together with the solid-phase free energies, can be used to construct a suitable EOS for the liquid.

In Sec. II we outline the model used to describe the solids (Sec. II A) and the liquid phase (Sec. II B). We describe in detail how the different parameters for the model are obtained from the first-principles calculations. In Sec. III, we discuss the resulting multiphase description. Finally, in Sec. IV, we briefly address the problem of connecting our multiphase carbon EOS to a Thomas Fermi-based model capable of describing behavior at extreme densities, both high and low, and at high temperatures.

II. CONSTRUCTION OF SINGLE-PHASE FREE ENERGIES

In what follows, we make the fundamental assumption that the Helmholtz free energy ($F=E-TS$) for each phase can be decomposed into three terms as

$$F(V,T) = F_0(V) + F_i(V,T) + F_e(V,T). \tag{1}$$

Here F_0 (the cold part), represents the ground-state energy for a system with *fixed* ionic positions, while the remaining two terms account for elementary excitations. The ion-thermal term, F_i, is the free energy due to lattice vibrations or other ionic excitations, and the electron-thermal term, F_e, is the free energy due to electronic excitations. Such a separation requires us to invoke the Born-Oppenheimer approximation, and the assumption that the modification of the free energy from electron-phonon coupling is small. Electron orbital occupancies are constrained to have a Fermi distribution at the equilibrium ionic temperature in the cases where this is potentially relevant, i.e., for the metallic liquid and semiconductor BC8 (but not for diamond as it has a large electronic gap, even at high temperatures).[27] In this way, we set the electron temperature equal to the ion temperature, so we are describing carbon in thermal equilibrium. The electronic structure calculations are performed within density-functional theory (DFT) using the generalized gradient approximation (GGA) of Perdew-Burke-Ernzerhof.[33] We use the pseudopotential approximation in the norm-conserving Troullier-Martins scheme.[34] Once the free energies of the individual phases are known, the standard two-phase Maxwell construction is used to determine phase lines for the system at constant pressure. This ensures that at a given set of (P,T) conditions, the favored phase is the one with the lowest Gibbs free energy. We now describe the construction of solid and liquid free energies in some detail.

A. Solid phases

Following Eq. (1), the free energy of each solid phase includes a cold piece given by DFT-GGA total-energy calculations of the crystalline system (diamond or BC8), in which the atoms are fixed in their equilibrium positions. This is done in a fcc (bcc) unit cell with two (eight) atoms for diamond (BC8), describing the electronic Kohn-Sham orbitals by a grid of $10\times10\times10$ $(3\times3\times3)$ k points and a plane-wave energy cutoff of 70 Ry. The BC8 basis vectors[35] are fully relaxed at each cell volume. We calculate the total energy on a grid of volumes for the two solid phases. A Vinet equation of state[36] is then fit to the DFT results to obtain a continuous function of volume (Fig. 2),

$$F_0(V) = \frac{4V_0B_0}{(B_0'-1)^2}[1-(1+X)\exp(-X)] + \phi_0, \tag{2}$$

where

$$X = \frac{3}{2}(B_0'-1)[(V/V_0)^{1/3}-1]. \tag{3}$$

This analytic form fits the computed points very well over a wide range of volumes[37] and allows us to extract the four

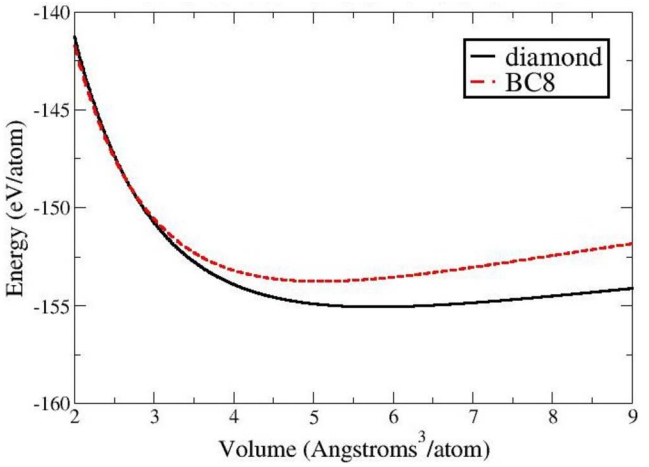

FIG. 2. (Color online) Vinet equation fits to the cold curves for diamond and BC8.

phase-dependent parameters: equilibrium volume V_0, bulk modulus B_0, pressure derivative of the bulk modulus B_0', and the minimum energy ϕ_0, which are reported in Table I. Note that the BC8 phase has an equilibrium volume slightly less than that of the diamond phase, and that the energies of the two phases converge as volume decreases. Furthermore, they cross at roughly a volume of ~2.68 Å^3/atom, corresponding to a pressure of 1075 GPa, after the effect of zero-point motion of the two phases is taken into account (see below). This is in agreement with previous theoretical predictions of the transition pressure at zero temperature using similar methods.[25] However, we note that our calculated V_0 for the diamond phase is 5.785 Å^3/atom, 3% larger than that of experiment once zero-point motion and thermal expansion have been accounted for. This is a well-known error resulting from the use of GGA-DFT. Depending on the intended application of the EOS, it may be necessary to shift V_0 "by hand" to bring it into exact agreement with experiment. For example, in designing dynamic high-pressure experiments, the final state achieved can be critically sensitive to the initial density. In what follows, we use our theoretical value for the sake of consistency and continuity.

For obtaining the ion-thermal term, F_i, we assume that the system is described well within the quasiharmonic approximation, together with small anharmonic corrections present at high temperatures. In quasiharmonic theory, the finite-T solid at a given density is modeled as a collection of noninteracting phonons.[38] The phonon spectrum depends on density so the phonon density of states, $D_V(\omega)$, is calculated as a function of V. We compute the full phonon dispersion and resulting phonon density of states within our GGA-DFT approach by the linear-response method as implemented in the ABINIT code.[39] For each solid phase, D_V is computed on a grid of volumes (normalized to unity by convention).

In principle, we can impose a Bose-Einstein distribution for the phonon modes and calculate the T-dependent quasiharmonic free energy at each V by performing the appropriate integral over $D_V(\omega)$. However, we need the free energy at a *continuous* set of volumes in order to compute the ion-thermal contribution to the pressure, for instance. Additionally, we aim to construct models in which the parameters have a very clear physical meaning. Since the frequency-dependent function $D_V(\omega)$ changes in subtle ways as V varies,[27] it may seem difficult to embody the V dependence in one or a few parameters. However, from the EOS point of view, the Debye-type models[40] provide an excellent approximation to the full quasiharmonic free energy. At high temperature, the Debye model free energy is within ~0.2% of the full quasiharmonic result if the Debye temperature, θ, is chosen to be θ_0 as defined by

$$k_B\theta_0(V) = \hbar e^{1/3} \exp\left(\int \log(\omega) D_V(\omega) d\omega\right). \tag{4}$$

In the same way, we define the ω^2 moment,

$$k_B\theta_2(V) = \sqrt{\frac{5}{3}\int (\hbar\omega)^2 D_V(\omega) d\omega}. \tag{5}$$

The high-temperature expansion of the quasiharmonic free energy can then be written as follows:[40]

$$F_h(V,T) = -3k_BT\left[\log\left(\frac{e^{1/3}T}{\theta_0(V)}\right) - \frac{1}{40}\left(\frac{\theta_2(V)}{T}\right)^2 + \cdots\right]. \tag{6}$$

In the opposite limit, as $T \to 0$, the harmonic free energy tends to $\frac{9}{8}k_B\theta_1$ (zero-point energy), where θ_1 is defined by

$$k_B\theta_1(V) = \frac{4}{3}\int \hbar\omega D_V(\omega) d\omega. \tag{7}$$

The three definitions for θ are equivalent for the ideal case of the Debye model [in which $D_V(\omega) \propto \omega^2$ for $\hbar\omega < \theta$ and is zero for $\hbar\omega > \theta$].[32]

TABLE I. Parameters for the carbon solid-phase equations of state. Volumes are in Å^3/atom, bulk moduli in GPa, energies in eV/atom, Debye temperatures in Kelvin, linear-volume Grüneisen coefficients (β) in Å^{-3} and anharmonic coefficients (a) in Kelvin^{-1}/atom. The $\theta^{(0)}$ are the values of θ at reference volumes, V_{ref}. V_{ref}(diamond)=5.571 Å^3/atom, and V_{ref}(BC8)=3.177 Å^3/atom. For each phase, $\theta(V) = \theta^{(0)}(\frac{V}{V_{ref}})^{-\alpha} \exp[\beta(V_{ref}-V)]$.

	Cold curve				Ion thermal									
					Harmonic									Anharmonic
	V_0	B_0	B_0'	ϕ_0	$\theta_A^{(0)}$	α_A	β_A	$\theta_B^{(0)}$	α_B	β_B	$\theta_0^{(0)}$	α_0	β_0	a
Diamond	5.785	368.2	4.038	−155.059	1887.8	0.913	−0.316	1887.8	0.429	0.168	1887.8	0.202	0.131	3.8×10^{-5}
BC8	5.077	539.7	3.821	−153.751	1961.9	0	0	3176.3	0.532	0.156	2727.27	0.131	0.192	5.5×10^{-5}

For many systems, θ_0 and θ_1 can be considered equal, which simplifies the description. For the diamond and BC8 phases of carbon, we find that θ_0 and θ_1 differ by more than 10% at high compressions. This is a result of the phonon density of states (PDOS) being rather different from the classic Debye form. As discussed in Ref. 27, the transverse-acoustic (TA) modes of diamond and BC8 are separated in energy from the rest of the phonon modes at high pressures, resulting in a double-peaked PDOS. In addition, these TA modes have energies, which are roughly independent of volume, unlike the remaining modes which exhibit a strong increase in energy upon compression. To represent this physics, we employ a "double-Debye" model, in which the PDOS is approximated by two overlapping Debye peaks, each of which is characterized by its own volume-dependent Debye temperature. The model PDOS as a function of volume then has the form

$$D_V(\omega) = \xi_A D_V^A(\omega) + \xi_B D_V^B(\omega), \tag{8}$$

where $D_V^{A,B}(\omega) \propto \omega^2$ for $\hbar\omega < k_B\theta_{A,B}$ (and zero otherwise) are the individually normalized Debye model phonon densities of states. The coefficients $\xi_{A,B}$ are determined by requiring that the total PDOS is normalized,

$$1 = \xi_A + \xi_B. \tag{9}$$

In addition to this constraint, we choose to require that the three phonon moments, θ_0, θ_1, and θ_2, be equal to those computed from the true PDOS at each volume,

$$\log(\theta_0) = \xi_A \log(\theta_A) + \xi_B \log(\theta_B), \tag{10}$$

$$\theta_1 = \xi_A \theta_A + \xi_B \theta_B, \tag{11}$$

$$\theta_2^2 = \xi_A \theta_A^2 + \xi_B \theta_B^2. \tag{12}$$

This gives us four nonlinear equations to determine the four unknowns (parameters of the PDOS model): ξ_A, ξ_B, θ_A, and θ_B, which must be solved *for each* volume at which the PDOS calculation was performed. In what follows, we stipulate that $\theta_A \leq \theta_B$. Using the normalization and θ_0 constraints, we can write

$$\xi_A = \frac{\log(\theta_B/\theta_0)}{\log(\theta_B/\theta_A)}, \quad \xi_B = \frac{\log(\theta_0/\theta_A)}{\log(\theta_B/\theta_A)}. \tag{13}$$

This implies that $\theta_A \leq \theta_0 \leq \theta_B$ if $\xi_{A,B}$ are to be greater than zero. The standard single-Debye model is recovered for the degenerate case $\theta_A = \theta_0 = \theta_B \equiv \theta$. The remaining two constraint equations for θ_1 and θ_2 can then be solved numerically to obtain θ_A and θ_B as functions of $(\theta_0, \theta_1, \theta_2)$. Figure 3 shows the PDOS of diamond at two representative volumes, together with the double-Debye fits for optimal values of the parameters. For the larger volume (close to ambient), the PDOS is well described by a single Debye model. The PDOS at the smaller volume, corresponding to a pressure above 1000 GPa, clearly shows two distinct contributions, which are described well with the double-Debye approach. Figure 4 shows the BC8 PDOS at two volumes, again with double-Debye fits. Figure 5 displays $\theta_A(V)$ and $\theta_B(V)$ for diamond and BC8. Note that for both phases, θ_A is roughly independent of volume; we assume it to be completely independent of V for BC8. This is consistent with the identification of the "A" peak as representing the TA modes.[27]

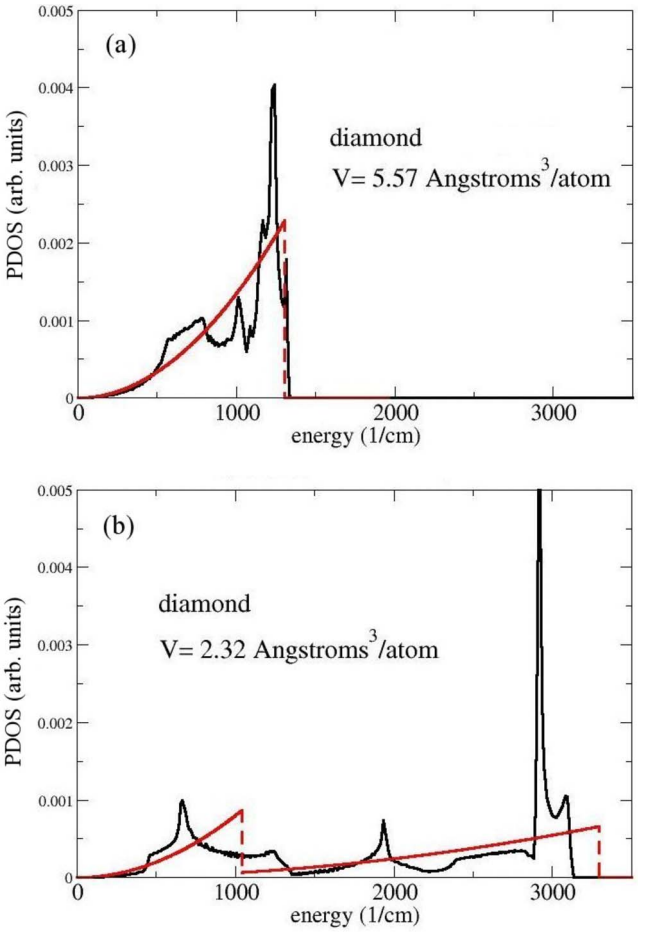

FIG. 3. (Color online) Phonon density of states of diamond for two different volumes: (a) 5.57 and (b) 2.32 Å^3/atom, together with the double-Debye model PDOS for those same volumes. Note that in (a) the model virtually reduces to that of a single-Debye model.

In order to characterize the V dependence of F_h, we must parametrize the V-dependence of the Debye temperatures. We do this by assuming that their respective Grüneisen parameters ($\gamma_{\{A,B,0\}}$) vary linearly with volume,

$$-\frac{d\log(\theta_{\{A,B,0\}})}{d\log(V)} \equiv \gamma_{\{A,B,0\}}(V) = \alpha_{\{A,B,0\}} + \beta_{\{A,B,0\}} V. \tag{14}$$

This form for the Grüneisen parameter allows us to satisfy a well-known infinite-compression limit derived for the one-component plasma if α is chosen to be $\frac{1}{2}$ (the plasma frequency of ions in a uniform negative compensating background $\propto V^{-1/2}$). Our calculated phonon moments, θ_0 and θ_1, for diamond and BC8 obtained directly from the PDOS are shown in Fig. 6 and are compared with θ_0 and θ_1 computed by our double-Debye model. The near-equality between the moments computed in the two different ways ensures the accuracy of the double-Debye approach. Note that the θ_0 are

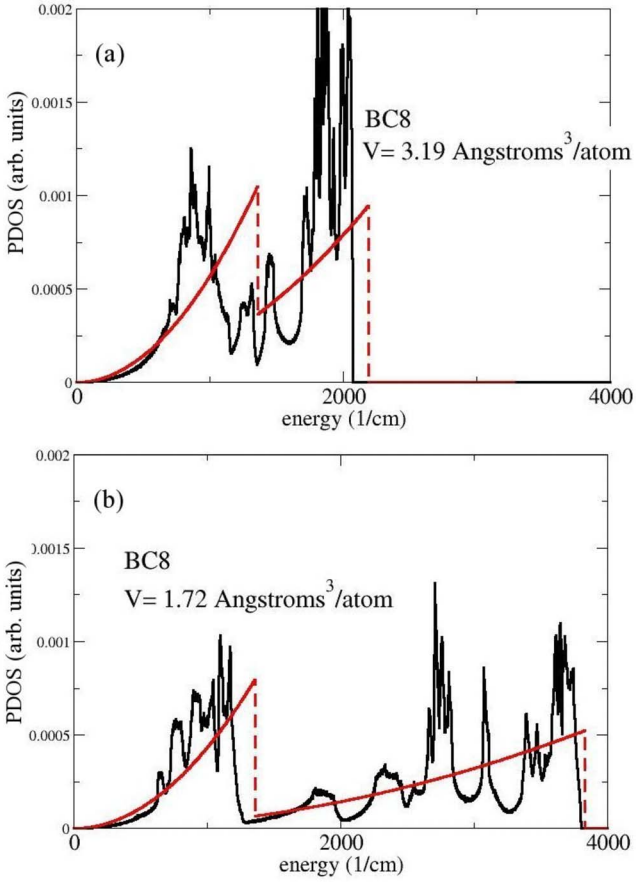

FIG. 4. (Color online) Phonon density of states of BC8 for two different volumes: (a) 3.19 and (b) 1.72 Å^3/atom, together with the double-Debye model PDOS for those same volumes.

roughly equal for the two solid phases throughout a range of volumes; this results in a diamond-BC8 transition pressure, which is only weakly dependent on temperature.[27]

The resulting harmonic free energy per atom is

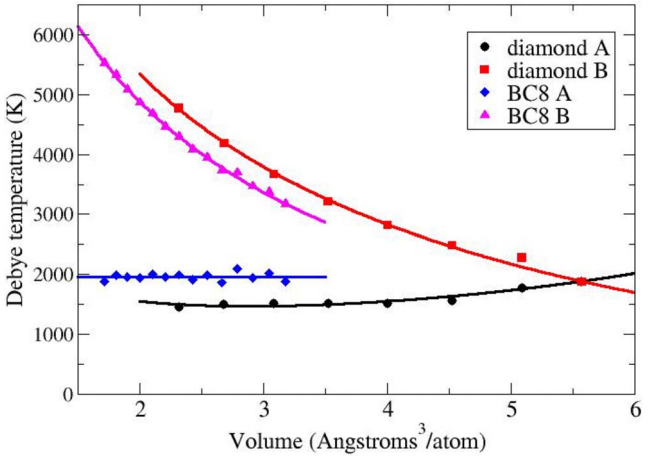

FIG. 5. (Color online) Debye temperatures θ_A and θ_B for diamond and BC8 phases at each volume (dots), together with fits assuming Grüneisen parameters which vary linearly with V (lines).

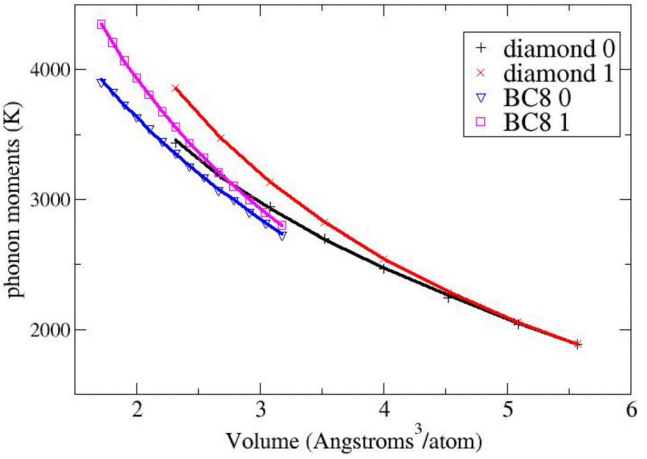

FIG. 6. (Color online) Phonon moments θ_0 and θ_1 for diamond and BC8 phases as computed directly from the PDOS (points), together with results from our double-Debye model (lines), assuming Grüneisen parameters which vary linearly with V.

$$F_h(V,T) = \frac{\log(\theta_B/\theta_0)}{\log(\theta_B/\theta_A)} f_h^A(V,T) + \frac{\log(\theta_0/\theta_A)}{\log(\theta_B/\theta_A)} f_h^B(V,T), \tag{15}$$

where the $f_h^{A,B}(V,T)$ are the classic single-Debye free energies,

$$f_h^{A,B} = k_B T \left\{ \frac{9}{8}\frac{\theta_{A,B}}{T} + 3\log\left[1 - e^{-\theta_{A,B}/T}\right] - \mathcal{D}\left(\frac{\theta_{A,B}}{T}\right) \right\}, \tag{16}$$

with

$$\mathcal{D}(y) = \frac{3}{y^3}\int_0^y \frac{x^3}{\exp(x)-1}dx. \tag{17}$$

From Eqs. (15) and (16), we see that the harmonic free energy is described in terms of the three characteristic temperatures: θ_A, θ_B, and θ_0, together with their respective Grüneisen parameters. The volume dependence of the quasiharmonic free energy of each phase is then fully described by the nine parameters: $\alpha_{\{A,B,0\}}$, $\beta_{\{A,B,0\}}$, and the integration constants $\theta^{(0)}_{\{A,B,0\}}$.

The standard single-Debye model is only capable of reproducing one moment (say, θ_0 *or* θ_1) and therefore cannot address both high- and low-T limits simultaneously. Our double-Debye model has the advantage that it reproduces both the zero-point energy and the quasiclassical limit ($T > \theta_0$). This is particularly important for diamond and BC8 carbon since (1) the characteristic phonon frequencies are high enough that zero-point motion is crucial even at ambient temperatures, and (2) at high pressures the low-T and high-T moments are quite unequal. We note that for T well above θ_0, the free energy (cold+ion thermal) reduces to that of the Mie-Grüneisen equation of state, for which $E(V,T) = F_0(V) + 3k_BT$ and $P(V,T) = P_0(V) + 3k_BT\gamma_0(V)/V$.

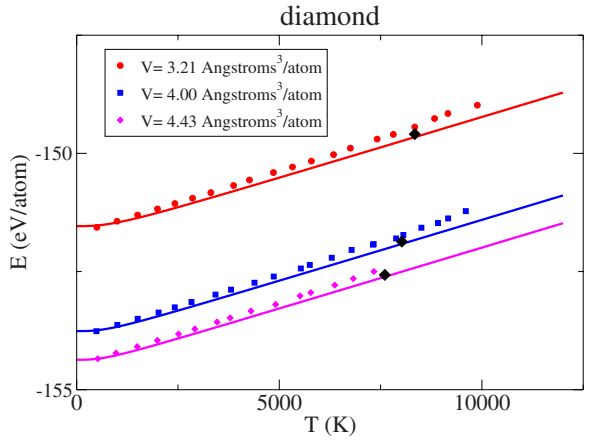

FIG. 7. (Color online) Diamond energy vs temperature obtained from averaging over constant-T constant-V molecular-dynamics trajectories (dots) and from quasiharmonic solid model (cold +quasiharmonic ion-thermal) (lines). The anharmonic term (not shown) is added later in order to bring the solid equation of state into agreement with the MD points. The diamonds indicate solidus temperature at the appropriate density, computed using our resulting multiphase EOS model.

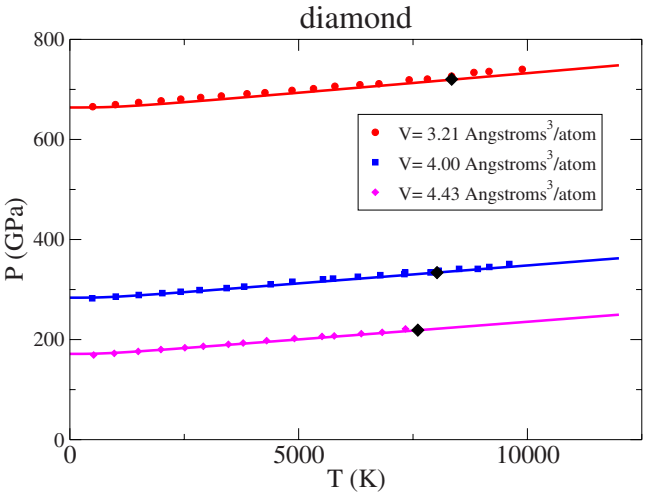

FIG. 8. (Color online) Diamond pressure vs temperature obtained from averaging over constant-T constant-V molecular-dynamics trajectories. In this case the quasiharmonic solid model (lines) reproduces the molecular-dynamics points with no added correction due to volume-independent anharmonic term (see text). The diamonds indicate solidus temperature at the appropriate density, computed using our resulting multiphase EOS model.

While the harmonic approximation is expected to be extremely reliable at low temperatures, it must begin to break down as T increases and should break down near melting, where the atomic vibration amplitudes become significant. Anharmonic perturbation-theory calculations[38] suggest that corrections to the ion-thermal free energy coming from anharmonicity are of the form $a_1(V)T^2+a_2(V)T^4+\cdots$. To investigate these effects, we have performed molecular dynamics (MD) within the GGA-DFT framework for both diamond and BC8 phases. The internal energy and pressure were computed by averaging over numerous uncorrelated snapshots during the MD runs, which involved periodically repeated cells of 64 (128) atoms for diamond (BC8). We use *ab initio* plane-wave Born-Oppenheimer MD with a 50 Ry energy cutoff and Γ-point k-point sampling. The instantaneous pressure of the system is defined as $P=-\partial E/\partial V+\rho k_B T$, where the partial derivative has an analytic expression within the first-principles implementation and T is the instantaneous (ion-kinetic) temperature.[41] Simulation times ranged from 1 to 5 ps with a time step of 0.5 fs. The system was weakly coupled to a velocity-scaling thermostat as implemented in the QBOX code.[42] Comparisons were then made to the energy and pressure as calculated by the EOS model constructed from the aforementioned cold and quasiharmonic ion-thermal terms (as explained below, electronic excitations for the solid phases were deemed to be of negligible importance).

Figures 7 and 8 show the internal energy and pressure, respectively, of the diamond phase along isochores as a function of temperature. We first note that the cold energy, $F_0(V)$, for the diamond phase had to be shifted up *rigidly* in energy by 0.0952 eV/atom to facilitate this comparison because the MD calculation was done at lower convergence than was used in computing the cold energy. (Roughly half of the discrepancy is due to number of k points and the other half is due to the energy cutoff.) The solid E and P model curves approach $T=0$ with zero slope; this is a result of zero-point motion present in the Debye model, but *not* in our MD, which treats the ions classically. So a fair comparison is only meaningful at somewhat higher T, in particular, above θ_1. Note that for the three volumes presented, E from the MD is larger at a given T than E from the model. This is the effect of anharmonicity. Subtracting the two results from each other, we find a difference of internal energies which is proportional to T^2 and is *roughly independent of volume*. An identical study was performed for BC8 with similar results, though unfortunately, a different shift in energy (0.18 eV/atom) was required to bring the MD and EOS model into correspondence, indicating that the convergence issues for BC8 and diamond are somewhat different. Thus, we have an anharmonic correction to the ion-thermal term of the free energy of the form

$$F_{\mathrm{i}}(V,T) = F_{\mathrm{h}}(V,T) - a(V)T^2 \tag{18}$$

for both solid phases, which is required if the internal energy is to have the deviation exhibited here. Since we find the corrections to be approximately volume-independent $[a(V) \equiv a]$, this implies no sizable anharmonic correction to the pressure $(P \equiv -\partial F/\partial V|_T)$; the close correspondence of MD and quasiharmonic model results in Fig. 8 bears this out. We find this to be approximately true for BC8 as well.

The final term considered for the solid-phase free energies is the contribution of thermally excited electrons. In the case of diamond, electronic excitations are not relevant because diamond has a large electronic gap that remains open even at finite temperatures and at the high pressures considered here, as has been shown in previous work.[27] The BC8 phase is a semiconductor at low pressures and is predicted to be a low-density-of-states metal at the range of compressions over which it is predicted to be stable.[19] Figure 9 shows our calculated (GGA-LDA) electronic density of states for BC8 at

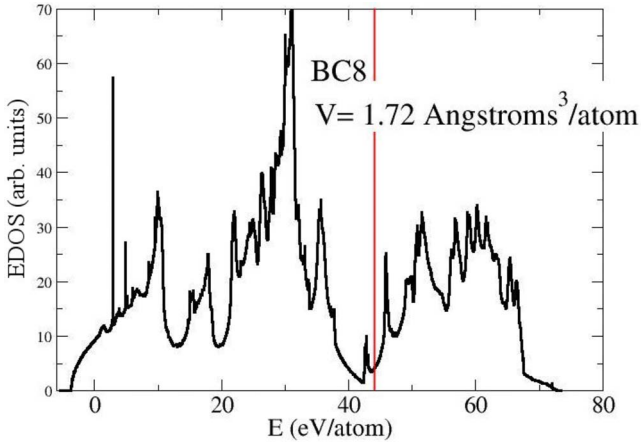

FIG. 9. (Color online) Electronic density of states of BC8 crystal for a volume of 1.72 Å^3/atom, corresponding to a pressure of 3685 GPa. The Fermi level is at 43.5 eV (vertical line), where the density of states is quite small.

high compression. For temperatures well below the Fermi temperature, T_F, the contribution of electronic excitations to the free energy can be computed by means of the Sommerfeld expansion.[38] This is an expansion of the free energy to order $(T/T_F)^2$, which includes the T-dependent change in the Fermi level while neglecting any T-dependent changes in the one-electron energies themselves, a fine approximation for $T \ll T_F$. In this approximation the electronic excitation term in the free energy is of the form $-\frac{1}{6}\pi^2(k_BT)^2N(E_F)$, where $N(E_F)$ is the density of states at the Fermi level. Since $N(E_F)$ depends on density, we again have the general form $F_e(V,T)=A(V)T^2$ [i.e., same form as the ion-anharmonic term of Eq. (18)]. Figure 10 shows $A(V)$ versus V for BC8 computed from our volume-dependent electronic density of states. Note the strong volume dependence resulting from the pressure-induced insulator-to-metal transition; even though the absolute values of $A(V)$ are quite small relative to those of good metals, we suspected that the strong V dependence

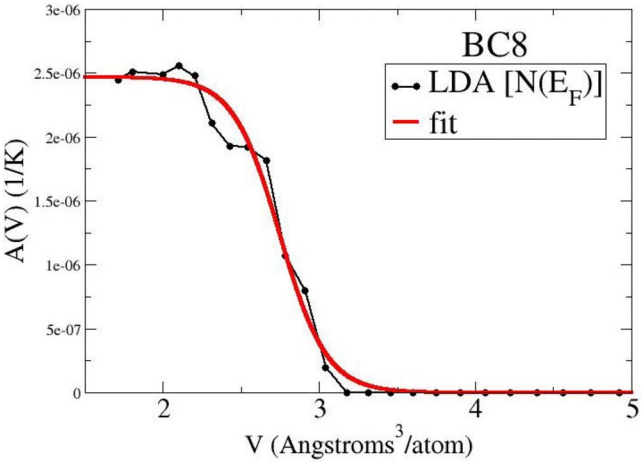

FIG. 10. (Color online) Density of states at the Fermi energy, $D(E_F)$, as a function of volume for BC8 phase. For low pressure this is effectively zero due to the presence of a finite electronic gap. The solid line is a smooth fit to the results (see text).

could result in a sizable contribution to the pressure. To wit, we fit our calculated results with the smooth curve shown in Fig. 10 and computed the resulting corrections to the thermal pressure. They are essentially negligible; small enough so that even the prediction of phase lines, which can be rather sensitive to small changes in free energy, will be unaffected. Thus, we conclude that electronic excitations are unimportant for the EOS of the solid phases of carbon in the range of our interest (below a pressure of ~2500 GPa).

Summarizing, the solid-phase free energies are obtained in three steps: First, the cold energies, $F_0(V)$, are computed and fit with smooth functions. Then the phonon densities of states are computed, along with the resulting Debye temperatures. A Debye-type model is constructed, again by fitting smooth functions to $\theta(V)$. Finally, the anharmonic term is added to bring the model results into correspondence with *ab initio* MD simulations of the pressure and internal energy. Electronic terms are ignored for diamond and BC8 phases due to their negligible contribution to the free energy. The parameters we use for our analytic free energy models for the solid phases are reproduced in Table I.

B. Liquid phase

The liquid EOS is more difficult to describe than that of the solid because there is no universally applicable model for liquid EOS analogous to the cold+quasiharmonic ion-thermal approach for solids. For the solid, the system can be thought of as moving about in configuration space in a single potential-energy well. The entropy in such a situation is then simply understood, which is why the solid-phase ion-thermal free energy can be accounted for in a Debye paradigm. Liquids, on the other hand, can at best be thought of as moving about on a complicated energy landscape possibly consisting of multiple distinct wells but certainly not confined to one or a few such wells. This makes a simple understanding of liquid entropy difficult if not impossible. MD, and/or Monte Carlo, simulations, which are directed at computing liquid free energies, are very computationally intensive because the system must be sampled over an enormous number of uncorrelated configurations in order to build up knowledge of the entropy. There are techniques available which attempt to minimize the computational cost of such calculations while still achieving high accuracy, such as potential switching integration.[43] Wang *et al.*[26] utilized this method to obtain the melting line of diamond. In general, liquid simulations, which are aimed at building up statistics required to obtain the free energy (so-called "thermodynamic integration" techniques), always make use of comparisons to reference states, for which the free energy is well known. These reference states could be analogous liquid systems with simpler interatomic force laws governing ionic motion (such as in potential switching), or they could be states of the same system at different thermodynamic conditions.

In this work, we make use of the diamond and BC8 melting curves computed previously[27] to constrain the free energy of the liquid, thereby using the solid free energies we determined above as references. These melting lines were obtained by direct simulation of the solid-liquid equilibrium

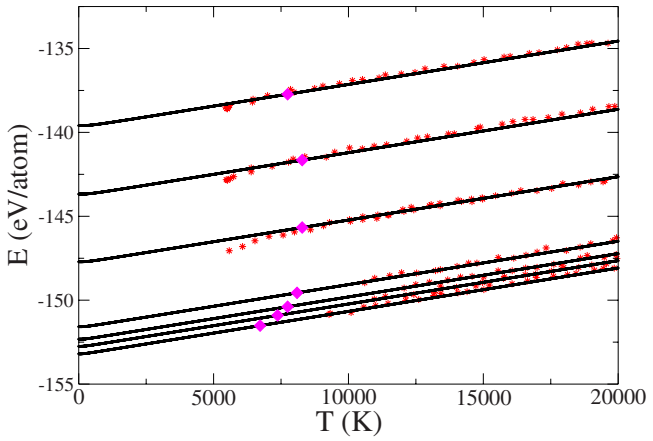

FIG. 11. (Color online) Liquid energy vs temperature obtained from averaging over constant-T constant-V molecular-dynamics trajectories (dots) and from liquid model (lines). Each curve corresponds to an isochore. From the bottom to the top of the figure, the volumes represented are 5.67, 4.93, 4.50, 4.00, 2.85, 2.31, and 1.98 Å^3/atom. The diamonds indicate liquidus temperature at the appropriate density, computed using our resulting multiphase EOS model.

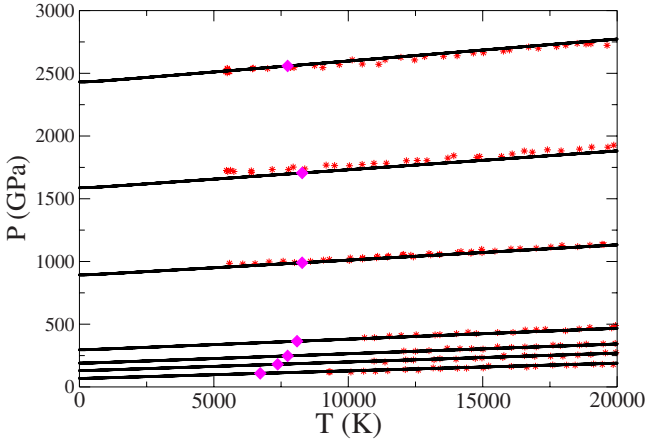

FIG. 12. (Color online) Liquid pressure vs temperature obtained from averaging over constant-T constant-V molecular-dynamics trajectories and from liquid model (lines). Each curve corresponds to an isochore. From the bottom to the top of the figure, the volumes represented are 5.67, 4.93, 4.50, 4.00, 2.85, 2.31, and 1.98 Å^3/atom. The diamonds indicate liquidus temperature at the appropriate density, computed using our resulting multiphase EOS model.

by means of the, so-called *two-phase method*.[44] Of note is the fact that the predicted diamond and BC8 melting temperatures both possess maxima as a function of pressure. The maximum in the diamond melting curve has been investigated previously in other theoretical work[26,27] and was inferred even before a direct calculation of the melting line was ever performed.[25] There has also been recent experimental confirmation of maxima in *both* diamond *and* BC8, although without the direct confirmation of the BC8 structure itself, with a laser compression technique coupled with *in situ* optical pyrometry.[45] Our previous simulations[27] on the melting lines of diamond and BC8 use the same underlying approximations as in this work. In a sense, the complex problem of obtaining the liquid entropy is then circumvented by making use of the melting lines, the determination of which rests on the fact that entropy *differences* (here, between solid and liquid) are easier to obtain than absolute values of liquid entropy.

In addition to the melting lines, we also directly compute the EOS (energy and pressure as a function of volume and temperature) in the liquid using *ab initio* MD. We perform MD on liquid carbon throughout a range of densities and temperatures corresponding to pressures of up to 3000 GPa and temperatures of more than twice T_{melt}. We use a simulation scheme similar to the one described Sec. II A with 64 atoms but with a time step lowered to 0.25 fs. As with the solid phases, we compute internal energy and pressure along isochores. Results are displayed in Figs. 11 and 12, together with the results of our liquid EOS model, discussed below. Well below T_{melt}, which is in the neighborhood of 8000 K for both solid phases, the liquid in the MD simulations is supercooled as is evidenced by a notable reduction in atomic diffusion. We disregard the E and P points with $T<10\,000$ K for this reason. Our first-principles MD results indicate that (1) $E(V,T)\sim F_0(V)+3k_BT$ and (2) $P(V,T)\sim P_0(V)+3k_BT\gamma/V$, with γ *roughly independent of volume* and equal to 0.84 ± 0.05. We thus feel justified in applying a solidlike free energy model to liquid carbon in this range of conditions. It is interesting that, even though we took care to include the effects of electronic excitations in the metallic liquid, the specific heat is essentially indistinguishable from $3k_B$ up to 20 000 K. Therefore, we do not include a T^2 term from either electronic excitations or "anharmonicity" in our liquid free energy.

To determine optimal values for $F_0(V)$ and $P_0(V)$ for the liquid, we extrapolate the MD data to $T=0$. This gives us F_0 and P_0 for seven values of V. We create a continuous "liquid cold curve" by fitting the largest four V with a Vinet form as in Eqs. (2) and (3) using the values $V_0=8.596$ Å^3/atom, $B_0=51.1$ GPa, $B_0'=5.85$, and $\phi_0=-153.651$ eV. We then introduce two corrections which bend the cold curve to fit the MD results for the three smallest volumes. These corrections are of the form

$$F_0(V)\rightarrow F_0(V)+\frac{K(V_1/V-1)^n}{L+(V_1/V-1)^n} \tag{19}$$

for $V<V_1$ and no correction for $V>V_1$. We apply two such corrections in succession. First, one at $V_1=3.9$ Å^3/atom, with $K=-5.0$ eV, $L=5.0$, and $n=3$ and then a second (*after* the first had been applied) at $V_1=2.7$ Å^3/atom, with $K=10.0$ eV, $L=3.0$, and $n=3$. The resulting $F_0(V)$, together with the assumptions $C_V=3k_B$ and $\gamma=0.84$, produces the model results shown as the black lines in Figs. 11 and 12. It should be noted that our resulting liquid cold curve possesses an effective bulk modulus which is significantly smaller than those of the two solid phases. This is encouraging since the liquid must be considerably more compressible than the solids in order for the melt temperatures to exhibit maxima as a function of presssure.[25–27] This is in contrast to melting in closed-packed elemental metals, in which the liquid is only

slightly more compressible than the solid and the resulting melt temperature increases monotonically with pressure.

Though this gives us an accurate representation of the liquid EOS (E and P as functions of V and T) throughout the range of pressures and temperatures of interest to us, we must still provide the elusive liquid entropy in order to facilitate free-energy matching between solid and liquid to constrain the melt lines. This necessitates adopting a liquid free-energy model, one which respects the above EOS, and possesses just enough freedom for us to tune the solid-liquid entropy difference in order to match the two-phase simulation results.[27] The liquid EOS model of Chisolm and Wallace,[31,32] developed for monatomic systems, is well suited to this task. It is based on an analogy between lattice vibrations of the crystalline solid and the atomic excitations of atoms in the massively multiwell potential of the liquid state. These authors hypothesize that the free energy (per atom) of the liquid has the following form:[46]

$$F(V,T) = F_0(V) + 3k_BT\log\left(\frac{\bar{\theta}}{T}\right) - k_BT\log(w) + F_e(V,T). \tag{20}$$

The rationale for this model is based on the observation that the specific heat of monatomic liquids is very close to $3k_B$ near melting and deviates from this value only as T is raised to many times the melting temperature, an observation borne out in our results above.[47] The first term corresponds to our hypothetical "cold curve," while the second term contains information about the curvature of the potential wells ("vibrational frequencies") through an effective Debye temperature. The third term accounts for the contribution of the existence of multiple wells to the configurational entropy, while the last term accounts for electronic excitations. Within this model, the number of distinct potential wells increases exponentially with the number of atoms in the system (w^N), so the contribution to the configurational entropy per atom is therefore $S_{\text{conf}}=k_B\log(w)$. The compatible mathematical forms of the second and third terms allow the constant w to be absorbed into a renormalized effective Debye temperature $\tilde{\theta}=\bar{\theta}/w^{1/3}$.

To give an idea of the physical meaning of $\tilde{\theta}$, it can be shown that the latent heat of melting is approximately $3k_BT_{\text{melt}}\log(\theta_{\text{sol}}/\tilde{\theta}_{\text{liq}})$ if anharmonicity and electronic contributions are small. This means that we can tune $\tilde{\theta}_{\text{liq}}$ to fit the solid-liquid entropy difference needed to accommodate our computed melting temperatures and internal energy differences. Though $\bar{\theta}_{\text{liq}}$ is meant to describe the curvature of a representative many-body potential well, we take this identification to be merely notional and use it instead as a "knob" for the entropy of the liquid.

With the specific heat, Grüneisen parameter, and cold curve fixed, we are left with one unknown: $\tilde{\theta}_0$, the renormalized effective Debye temperature at a *fixed* volume [the volume dependence having been fixed by our choice of $\gamma(V)\sim 0.84$]. We find that the value $\tilde{\theta}_0(V_{\text{ref}}=6.695\ \text{Å}^3/\text{atom})=520$ K allows us to best match the two-phase simulation melt curves. Figure 13 shows the phase diagram of our model, together with the two-phase results. Note that the low-P portion of the melt curve is extremely well reproduced, while the higher pressures less so. In particular, our triple point is somewhat different from that suggested by the two-phase simulations, resulting from the diamond and BC8 melt curves of our model possessing less curvature at higher pressures. Also, our BC8 melt temperature is slightly too high at $P=2000$ GPa. We stress that the determination of phase lines is extremely sensitive to very small changes in the EOS of the individual phases. At higher pressures, this is even more the case, as the surfaces of competing phases become more similar. We submit that this is the best we can do in fitting the melt lines, subject to the requirement of obtaining an accurate match to the liquid MD EOS as shown in Figs. 11 and 12.

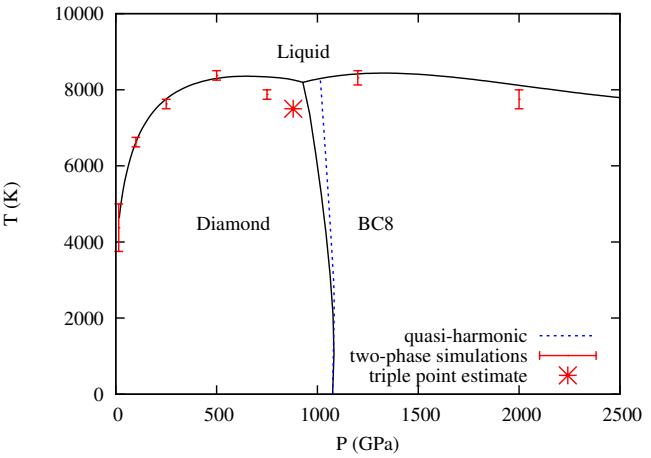

FIG. 13. (Color online) Phase diagram for carbon as obtained from the free energies described in this work (solid black) compared with melting curve (red error bars) of the two-phase simulations (extracted from Ref. 27). The diamond-BC8 phase line can be compared to the one resulting from neglecting anharmonic terms in both phases (dotted blue); this curve is shown to illustrate the effect of anharmonicity in the solid-solid-phase line. The slightly larger anharmonic term in the BC8 phase results in the entropy of that phase being slightly greater than the entropy of diamond, causing BC8 to be slightly favored as T is increased. This moves the triple-point to lower P and lower T when compared with that resulting from harmonic-only free energies.

III. MULTIPHASE EQUATION OF STATE MODEL: DISCUSSION

The parameters that describe the free energy of the solid phases are summarized in Table I, together with the discussion of Sec. II, which describes the liquid free energy. Model phase lines are computed using the two-phase tangent Maxwell construction, in which the transition pressure, between phases 1 and 2, P_{12}, and transition volumes, V_1 and V_2, are computed from the equation

$$F_1(V_1,T) - F_2(V_2,T) = -P_{12}(V_2 - V_1). \tag{21}$$

To describe the mixed phase region between V_1 and V_2, additional hypotheses need to be made; we take the free energy

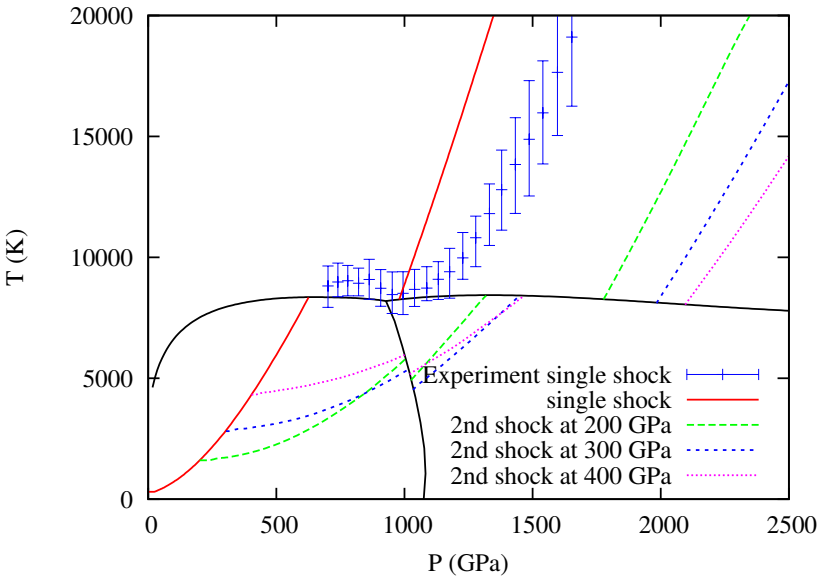

FIG. 14. (Color online) Hugoniot curves of carbon in (P,T)-space as calculated from our EOS model, initial condition in the diamond state, and extensions to BC8 and liquid phase. The full line (red) is the diamond primary Hugoniot (calculated with an initial state at ambient condition). Note that primary Hugoniot does not reach BC8 region of stability. The dashed lines indicate secondary Hugoniot with a second shock started at 200, 300, and 400 GPa. The blue crosses are the data of Ref. 45. The black lines are the coexistence and melting lines.

to be a volume-weighted average of single-phase free energies,

$$F(V,T) = (1-\lambda)F_1(V,T) + \lambda F_2(V,T), \tag{22}$$

where $\lambda = (V-V_1)/(V_2-V_1)$. This corresponds to the ideal picture of a homogeneous mixture of phases 1 and 2 with no sizable interfacial free energy for regions separating the phases. While this approximation may not be strictly justified, it provides a simple and practical means for generating a multiphase EOS table for use in hydrodynamic simulations where coexistence situations are reached. The phase diagram resulting from the application of Eq. (21) is shown in Fig. 13. We have already discussed the melting lines above; we now note that the diamond-BC8 phase line is slightly affected by the anharmonic terms we took care to include in the solid phases (see Fig. 13).

Experiments on carbon in extreme conditions fall into several categories. First, there are ambient pressure properties as a function of temperature, such as thermal expansion and the low-pressure melting temperature. We find a thermal-expansion parameter (at $P=0$ and $T=300$ K) of 1.7×10^{-6} K^{-1},[48] in qualitative agreement with the experimental value of 1.0×10^{-6} K^{-1}.[49] This small value is a result of the large bulk modulus and the small Grüneisen parameter in the diamond phase. The low-P diamond melting temperature of our multiphase model shown in Fig. 13 is in excellent agreement with the first-principles GGA-DFT predicted value of 4000 or 4500 K of Refs. 27 and 26 and the experimental extrapolated value of 3820 K. We note that this has been facilitated by our choice of liquid Debye temperature.

Second, there are shock measurements on the diamond phase. These are of the form: final density versus shock pressure, given ambient initial conditions, after the usual translation is made from the u_s and u_p variables (shock speed and particle speed). The bulk of these data is from the work of Pavlovskii.[50] If we assume that these measurements correspond to states along the principal Hugoniot of diamond, we obtain excellent agreement with their measured points in (ρ,P) space, provided that we shift our diamond V_0 slightly so as to coincide with the experimental value.

Third, there are recent measurements on the Hugoniot in the liquid phase,[45] in which the inferred quantities include pressure and temperature (optical pyrometry being possible from the liquid since it is metallic). These experimental data consist of two distinct parts. There is a plateau region where the shock temperature is roughly constant with pressure between 550 and 1100 GPa (see Fig. 14). It corresponds well to our diamond melting line in this pressure range and the hints of a maximum in the diamond melting curve, though the experimental value of T in the plateau region is $\sim$1500 K higher than our melting temperatures.[51] Thus, we assume that these points correspond to states in the diamond-liquid mixed phase region. The second part includes the data where the shock temperature grows rapidly with pressure for $P > 1100$ GPa. This is the Hugoniot in the liquid (again, with an ambient diamond initial condition). At a given pressure, we calculate the liquid Hugoniot to have a temperature significantly higher than the that of the experiment. Our liquid Hugoniot,[52] displayed along with the measurement[45] in Fig. 14, is in rough agreement with that of similar work by Romero *et al.*[53] Although our liquid EOS model is somewhat approximate, we find it difficult to explain this large disagreement with the experimental results. The offset in (P, T) space between the solid and liquid branches of the principal Hugoniot reflects the difference in entropy, and therefore latent heat, between solid and liquid. Our results suggest $\Delta S_{\mathrm{melt}} \sim 2.9 k_B$ per atom along an isochore in the vicinity of shock melting, while our modeling of the experimental results suggests a value of roughly $4.5 k_B$ per atom. In a theoretical work, Wang *et al.*[26] reported $\Delta S_{\mathrm{melt}} \sim 2.5 k_B$. Further theoretical and experimental work must be done to resolve this discrepancy.

IV. EQUATION OF STATE EXTENSION TO THE PLASMA LIMIT

To apply the multiphase EOS model to simulations of very high-energy-density laser-fusion experiments on the

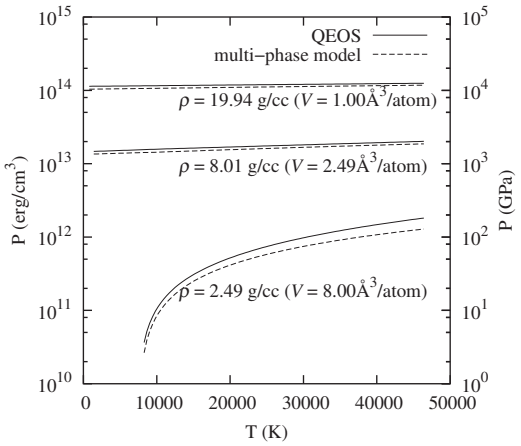

FIG. 15. Comparison of multi-phase and QEOS carbon isochores at the boundaries of the multiphase region.

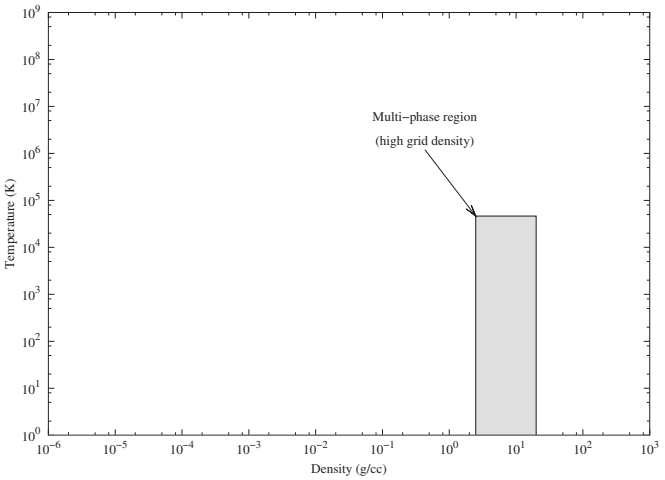

FIG. 16. The EOS table generated (ρ,T) grid used in the hydrodynamic simulations. The multiphase region (as constructed in Secs. II and III) is shaded, while the rest is described by the QEOS model.

National Ignition Facility (NIF) at Livermore, we need to extend the EOS to much wider ranges of density and temperature. High-intensity laser light on a diamond surface will produce strong compressive shocks as well as ablation of hot vapor.

Simulation of NIF experiments with hydrodynamic codes requires the pressure and energy functions in tabular format, in which the independent variables are mass density (ρ) and temperature (T). We generate the final carbon EOS table by embedding a table produced from the multi-phase model (explained in the previous sections) into a much larger-range table produced by the QEOS model.[54] In order to represent accurately the latent heat of melting in diamond, a very finely gridded table is needed. The multiphase model is used to generate a rectangular (ρ,T) table over the range $2.49 \leq \rho \leq 19.94$ g/cm^3 and $1 \leq T \leq 46,420$ K. The table grid contains 400 densities and 300 temperatures with a logarithmic spacing. This grid allows for good definition of the melting transition and its latent heat.

In the QEOS code, the thermodynamic functions are partitioned as in Eq. (1). The cold curve is the Thomas-Fermi cold isotherm plus a two-parameter function that guarantees the correct experimental values of reference density and bulk modulus. The ionic term represents the solid and fluid phases, separated by a Lindemann model melting curve. The solid model is a Debye model. The fluid model has an ion heat capacity of $3k_B$ at the melting boundary and drops to $3/2k_B$ at high temperatures according to the scaling law $[T_{\rm melt}(\rho)/T]^{1/3}$, where $T_{\rm melt}(\rho)$ is the Lindemann melting temperature prediction. The QEOS melting curve is only a model boundary and has no latent heat of melting. The Lindemann melting line used in QEOS is only a means to construct the liquid specific heat, and it does not affect in any way our explicit melting lines described earlier in the multiphase model region. The electronic term is given by the Thomas-Fermi model. These models are designed to give accurate physics behavior at the low and high limits of temperature and density. For intermediate (ρ,T) conditions, the cold curve and ionic models are parametrized to allow fits to a wide variety of materials.[54,55] We use adjustable parameters[54] in the cold-curve pressure and in the Grüneisen function $\gamma(\rho)$ to make a best fit to the multiphase pressure isotherms at high and low temperatures so that the tables will merge smoothly along the boundaries. QEOS and multiphase pressure isochores are compared in Fig. 15. The fit is not perfect but is adequate for generating the large EOS table. The QEOS code was then run to produce a table over the range $10^{-6} \leq \rho \leq 10^3$ g/cm^3 and $1 \leq T \leq 10^9$ K, which also includes the same (ρ,T) grid used in the multiphase model.

The two tables are then merged by replacing the QEOS data in the multiphase model (ρ,T) range with the multiphase data. The discontinuities along the boundaries of the multiphase and QEOS regions are small and can be smoothed out by table interpolation. The resulting table contains nearly 200000 points. The total (ρ,T) region is compared with the multiphase model region in Fig. 16. Preliminary hydrodynamic simulations have been carried out with the resulting EOS table and are currently being used in the design of carbon-based fusion capsules for the NIF.[56]

V. CONCLUSIONS

We have constructed a multiphase equation of state for carbon at high pressures entirely from first-principles calculations. The solid-phase free energies include the effects of quantum ions at low temperatures through a Debye-type treatment and anharmonic effects at high temperatures. The melting lines, also calculated by first-principles electronic structure methods, served effectively as a reference for the construction of the liquid equation of state. A simple form for the free energy of the liquid, based on a picture for monatomic systems, was assumed and was shown to reproduce the general features of our *ab initio* molecular-dynamics calculations of liquid EOS, while reproducing the maxima in the melting lines for both diamond and BC8. We also employed a prescription for connecting the detailed multiphase EOS model to a Thomas-Fermi model aimed at addressing extreme densities and temperatures. The chain of calculations from first-principles molecular dynamics, to multiphase

free energy models, to EOS tables, and to hydrodynamic simulations represents a step forward in applied physics. This prescription is expected to be useful for many other materials of interest that may be subjected to high-energy-density conditions.

We note that there are still a few troubling issues regarding the comparison to experiments on carbon. Most notably, our predictions of the principal Hugoniot in the liquid phase are discrepant from recent laser-driven shock measurements.[45] Additional experimental and theoretical work will most likely be needed in order to address this issue and to shed further light on the amount of latent heat involved in the diamond-to-liquid transition.

ACKNOWLEDGMENTS

We thank G. W. Collins, J. Eggert, D. G. Hicks, D. Orlikowski, D. Ho, D. H. Munro, S. W. Haan, F. H. Ree, M. van Thiel, N.A. Romero, and R. E. Rudd for helpful discussions. This work was performed under the auspices of the U.S. Department of Energy at the Lawrence Livermore National Laboratory under Contract DE-AC52-07NA27344.

[1] D. K. Bradley, J. H. Eggert, D. G. Hicks, P. M. Celliers, S. J. Moon, R. C. Cauble, and G. W. Collins, Phys. Rev. Lett. **93**, 195506 (2004).
[2] H. Nagao, K. G. Nakamura, K. Kondo, N. Ozaki, K. Takamatsu, T. Ono, T. Shiota, D. Ichinose, K. A. Tanaka, K. Wakabayashi, K. Okada, M. Yoshida, M. Nakai, K. Nagai, K. Shigemori, T. Sakaiya, and K. Otani, Phys. Plasmas **13**, 052705 (2006).
[3] S. L. Johnson, P. A. Heimann, A. G. MacPhee, A. M. Lindenberg, O. R. Monteiro, Z. Chang, R. W. Lee, and R. W. Falcone, Phys. Rev. Lett. **94**, 057407 (2005).
[4] B. A. Hammel and the National Ignition Campaign Team, Plasma Phys. Controlled Fusion **48**, B497 (2006).
[5] M. A. Meyers, *Dynamic Behavior of Materials* (Wiley, New York, 1994).
[6] M. Ross, Nature (London) **292**, 435 (1981).
[7] W. B. Hubbard, Science **214**, 145 (1981).
[8] L. R. Benedetti, J. H. Nguyen, W. A. Caldwell, H. Liu, M. Kruger, and R. Jeanloz, Science **286**, 100 (1999).
[9] L. M. Ghiringhelli, C. Valeriani, E. J. Meijer, and D. Frenkel, Phys. Rev. Lett. **99**, 055702 (2007).
[10] J. S. Albinson and A. Evans, Astrophys. Space Sci. **131**, 443 (1987).
[11] J. L. Barrat, J. P. Hansen, and R. Mochkovitch, Astron. Astrophys. **199**, L15 (1988).
[12] P. Dufour, J. Liebert, G. Fontaine, and N. Behara, Nature (London) **450**, 522 (2007).
[13] L. Segretain, G. Chabrier, M. Hernanz, E. Garcia-Berro, J. Isern, and R. Mochkovitch, Astrophys. J. **434**, 641 (1994).
[14] T. S. Metcalfe, M. H. Montgomery, and A. Kannan, Astrophys. J. **605**, L133 (2004).
[15] Marc J. Kuchner and Sara Seager, arXiv:astro-ph/0504214 (unpublihsed).
[16] S. Seager, M. Kuchner, C. A. HierMajumder, and B. Militzer, Astrophys. J. **669**, 1279 (2007).
[17] In principle, dynamic compression could involve time scales fast enough so that equilibrium is not reached, in which case detailed kinetic models would have to be employed. We ignore these effects in this work.
[18] We ignore the graphite phase in this work. In particular, we envision a scenario in which dynamic compression is applied to a diamond-phase initial state.
[19] S. Fahy and S. G. Louie, Phys. Rev. B **36**, 3373 (1987).
[20] M. T. Yin and M. L. Cohen, Phys. Rev. Lett. **45**, 1004 (1980).
[21] G. I. Kerley and L. Chhabildas, Sandia National Laboratories Report No. SAND2001-2619, 2001.
[22] M. van Thiel and F. H. Ree, Phys. Rev. B **48**, 3591 (1993).
[23] A. M. Molodets, Fiz. Goreniya Vzryva **34**, 94 (1998).
[24] F. P. Bundy, W. A. Bassett, M. S. Weathers, R. J. Hemley, H. U. Mao, and A. F. Goncharov, Carbon **34**, 141 (1996).
[25] M. P. Grumbach and R. M. Martin, Phys. Rev. B **54**, 15730 (1996).
[26] X. Wang, S. Scandolo, and R. Car, Phys. Rev. Lett. **95**, 185701 (2005).
[27] A. A. Correa, S. A. Bonev, and G. Galli, Proc. Natl. Acad. Sci. U.S.A. **103**, 1204 (2006).
[28] S. Brygoo, E. Henry, P. Loubeyre, J. Eggert, M. Koening, B. N. Loupias, A. Bebuzzi, and M. R. Le Gloahec, Nat. Mater. **6**, 274 (2007).
[29] L. E. Fried and W. M. Howard, Phys. Rev. B **61**, 8734 (2000).
[30] K. V. Khishchenko, V. E. Fortov, and I. V. Lomonosov, Int. J. Theor. Phys. **26**, 479 (2005).
[31] E. D. Chisolm and D. C. Wallace, J. Phys. C **13**, R739 (2001).
[32] E. D. Chisolm, S. D. Crockett, and D. C. Wallace, Phys. Rev. B **68**, 104103 (2003).
[33] J. P. Perdew, K. Burke, and M. Ernzerhof, Phys. Rev. Lett. **77**, 3865 (1996).
[34] N. Troullier and J. L. Martins, Phys. Rev. B **43**, 1993 (1991).
[35] J. Crain, S. J. Clark, G. J. Ackland, M. C. Payne, V. Milman, P. D. Hatton, and B. J. Reid, Phys. Rev. B **49**, 5329 (1994).
[36] P. Vinet, J. H. Rose, J. Ferrante, and J. R. Smith, J. Phys. C **1**, 1941 (1989).
[37] We fit the cold curve over a wide range of volumes ($\sim$1–9 Å^3/atom), so we do not expect our extracted cold-curve parameters (V_0, B_0, B_0', and ϕ_0) to be the optimal ones for describing the behavior *right in the neighborhood of* V_0 (i.e., near ambient conditions). Rather, they are a set of parameters which give a good *global* fit over the wide range of volumes considered.
[38] D. C. Wallace, *Thermodyamics of Crystals* (Dover, New York, 1998).
[39] ABINIT is a common project of the Universite Catholique de Louvain (Louvain-la-Neuve, Belgium), Corning Incorporated, and other contributors.
[40] D. C. Wallace, Phys. Rev. E **56**, 1981 (1997).
[41] O. H. Nielsen and R. M. Martin, Phys. Rev. B **32**, 3792 (1985).
[42] QBOX is a C++/MPI scalable parallel implementation of first-principles molecular dynamics (FPMD) based on the plane-wave pseudopotential formalism developed by F. Gygi (http://eslab.ucdavis.edu/).

[43] D. Frenkel and B. Smit, *Understanding Molecular Simulation* (Academic, San Diego, 2002).
[44] J. R. Morris, C. Z. Wang, K. M. Ho, and C. T. Chan, Phys. Rev. B **49**, 3109 (1994).
[45] J. H. Eggert, D. G. Hicks, P. M. Celliers, D. K. Bradley, S. R. McWilliams, R. Jeanloz, J. E. Miller, T. R. Boehly, and G. W. Collins (unpublished).
[46] There should also be terms accounting for the system making a transition from one distinct well to another. We assume that the system spends most of its time in individual wells rather than between them, in which case these terms are small (Ref. 31).
[47] At very high temperatures (many times T_{melt}), ion kinetic energy dominates over interion potential energy and the system behaves like an ideal gas with $E \sim \frac{3}{2} k_B T$. This is taken into account in our plasma-based model.
[48] Our agreement would be significantly better if we used a diamond bulk modulus and a Grüneisen parameter from experiment to fit our EOS since the thermal-expansion coefficient involves the ratio of these two quantities. Part of the discrepancy is therefore due to our adherence to the first-principles results for this study, together with the fact that our bulk modulus was taken from a fit to a wide range of volumes (rather than just in the neighborhood of V_0). We feel this is of little concern, however, since thermal expansion for diamond is so small (for most materials it is an order of magnitude larger). Thus, our final EOS: $E=E(V,T)$, $P=P(V,T)$ should still be quite accurate.
[49] G. A. Slack and S. F. Bartram, J. Appl. Phys. **46**, 89 (1975).
[50] M. N. Pavlovskii, Sov. Phys. Solid State **13**, 741 (1971).
[51] Uncertainty of this magnitude is to be expected from the prediction of melting temperatures using DFT-based methods.
[52] We determined the solid and liquid Hugoniots of Fig. 14 by taking the initial density to be that of experiment at ambient conditions ($P=0$, $T=300$ K). Since the ambient density of our EOS model is slightly shifted from this (due to the GGA-DFT error), our starting pressure is nonzero ($\sim$12 GPa). Alternatively, we could have chosen the same experimental starting density but required $P=0$. This would have shifted the curves in temperature. If we use this prescription, the resulting solid and liquid Hugoniots are shifted up in pressure (relative to those displayed) by roughly 20 GPa near shock-melting. This is a very small shift compared to the theory-experiment liquid Hugoniot disagreement we discuss here.
[53] N. A. Romero and W. D. Mattson, Phys. Rev. B **76**, 214113 (2007).
[54] D. A. Young and E. M. Corey, J. Appl. Phys. **78**, 3748 (1995).
[55] R. M. More, K. H. Warren, D. A. Young, and G. B. Zimmerman, Phys. Fluids **31**, 3059 (1988).
[56] D. Ho (private communication).